Loss of TDP-43 in astrocytes leads to motor deficits by triggering A1-like reactive phenotype and triglial dysfunction

Audrey Yi Tyan Peng[a,1], Ira Agrawal[a,1], Wan Yun Ho[a,1], Yi-Chun Yen[a,2], Ashley J. Pinter[a], Jerry Liu[a], Qi Xuan Cheryl Phua[a], Katrianne Bethia Koh[a], Jer-Cherng Chang[a], Emma Sanford[a], Jodie Hon Kiu Man[a], Peiyan Wong[b,c], David H. Gutmann[d], Greg Tucker-Kellogg[e,f], and Shuo-Chien Ling[a,c,g,3]

[a]Department of Physiology, Yong Loo Lin School of Medicine, National University of Singapore, 117549 Singapore, Singapore; [b]Department of Pharmacology, Yong Loo Lin School of Medicine, National University of Singapore, 117600 Singapore, Singapore; [c]Program in Neuroscience and Behavior Disorders, Duke–NUS Medical School, 169857 Singapore, Singapore; [d]Department of Neurology, Washington University School of Medicine in St. Louis, St. Louis, MO 63110; [e]Computational Biology Programme, Faculty of Science, National University of Singapore, 117558 Singapore, Singapore; [f]Department of Biological Sciences, Faculty of Science, National University of Singapore, 117558 Singapore, Singapore; and [g]Centre for Healthy Longevity, National University Health System, 117549 Singapore, Singapore

Edited by Junying Yuan, Harvard Medical School, Boston, MA, and approved September 24, 2020 (received for review April 22, 2020)

Patients with amyotrophic lateral sclerosis (ALS) can have abnormal TDP-43 aggregates in the nucleus and cytosol of their surviving neurons and glia. Although accumulating evidence indicates that astroglial dysfunction contributes to motor neuron degeneration in ALS, the normal function of TDP-43 in astrocytes are largely unknown, and the role of astroglial TDP-43 loss to ALS pathobiology remains to be clarified. Herein, we show that TDP-43–deleted astrocytes exhibit a cell-autonomous increase in GFAP immunoreactivity without affecting astrocyte or microglia proliferation. At the transcriptomic level, TDP-43–deleted astrocytes resemble A1-reactive astrocytes and induce microglia to increase C1q expression. These astrocytic changes do not cause loss of motor neurons in the spinal cord or denervation at the neuromuscular junction. In contrast, there is a selective reduction of mature oligodendrocytes, but not oligodendrocyte precursor cells, suggesting triglial dysfunction mediated by TDP-43 loss in astrocytes. Moreover, mice with astroglial TDP-43 deletion develop motor, but not sensory, deficits. Taken together, our results demonstrate that TDP-43 is required to maintain the protective functions of astrocytes relevant to the development of motor deficits in mice.

amyotrophic lateral sclerosis (ALS) | TDP-43 | cell-autonomous | A1-reactive astrocytes | triglial dysfunction

In neurodegenerative diseases, such as Alzheimer's disease (AD), the pathological hallmarks of the condition are often characterized by the aberrant aggregation of proteins encoded by mutant genes that cause the rarer familial forms of the disease. In this regard, ∼50 mutations have been identified in the *TARDBP* gene, encoding the TDP-43 protein, which is linked to amyotrophic lateral sclerosis (ALS) and frontotemporal dementia (FTD) (1–4). Moreover, intracellular inclusions containing TDP-43 proteins are present in the brains and spinal cords of >90% of sporadic ALS and ∼45% of FTD patients (5–7). This TDP-43 gene–pathology relationship in ALS and FTD suggests a critical role for TDP-43 in ALS/FTD pathogenesis. Intriguingly, the characteristic TDP-43 histopathology is the presence of cytoplasmic TDP-43 inclusions accompanied by a clearance of nuclear TDP-43 and intranuclear TDP-43 inclusions in both neurons and glial cells (8–10). As such, loss of normal nuclear TDP-43 function in neurons or glia could contribute to ALS/FTD and other TDP-43 proteinopathy-related diseases (7, 11).

TDP-43 is a 414-amino acid nucleic-acid binding protein containing an N-terminal ubiquitin-like fold and two RNA recognition motifs, followed by a glycine-rich, low-sequence complexity prion-like domain at the C terminus. Although TDP-43 was originally described to harbor transcription repressor activity (12), the functions of TDP-43 has since been expanded to include a wide range of biological processes (7, 13–15), including biogenesis and processing of coding and noncoding RNAs (7, 13–15), mRNA transport (16), translation (17, 18), mitochondrial function (19), autophagy (20, 21), and organelle homeostasis (22). While TDP-43 is expressed in all major cell types within the central nervous system (CNS) (23), it is not known whether TDP-43 has cell-type–specific functions.

Within the CNS, glia are viewed as supporting cells that provide an optimal environment for neurons to function properly (24). However, recent studies have highlighted more "active" roles of glia in brain health (25, 26). For example, astrocytes can form scars that aid axon regeneration (27) or become reactive, known as "A1"-reactive astrocytes, to kill neurons and oligodendrocytes (28). Critically, blocking the transitions to A1 astrocytes is effective in ameliorating neurodegeneration in AD and Parkinson's disease

Significance

Aberrant TDP-43 aggregation is one of the defining pathological hallmark proteins of two overlapping adult-onset neurodegenerative diseases, amyotrophic lateral sclerosis and frontotemporal dementia. While TDP-43 aggregates are also found in astrocytes, it is not known how loss of astroglial TDP-43 affects neuronal function and disease pathogenesis. Herein, we show that TDP-43 is required for maintaining the protective properties of astrocytes, such that loss of astroglial TDP-43 causes triglial abnormalities that result in motor deficits. These findings establish that TDP-43–mediated dysfunction in different cell types uniquely contributes to neurodegenerative disease through cell-type–specific mechanisms. Delineating these etiologies could facilitate the discovery of novel strategies to treat neurological disorders caused by TDP-43 proteinopathy.

Author contributions: A.Y.T.P., I.A., W.Y.H., Y.-C.Y., A.J.P., J.L., J.H.K.M., P.W., G.T.-K., and S.-C.L. designed research; A.Y.T.P., I.A., W.Y.H., Y.-C.Y., A.J.P., J.L., Q.X.C.P., K.B.K., J.-C.C., E.S., P.W., and S.-C.L. performed research; A.Y.T.P., I.A., W.Y.H., D.H.G., G.T.-K., and S.-C.L. contributed new reagents/analytic tools; A.Y.T.P., I.A., W.Y.H., Y.-C.Y., A.J.P., J.L., Q.X.C.P., K.B.K., J.-C.C., E.S., P.W., G.T.-K., and S.-C.L. analyzed data; D.H.G. edited the manuscript for grammar and flow; and I.A., W.Y.H., and S.-C.L. wrote the paper.

The authors declare no competing interest.

This article is a PNAS Direct Submission.

[1]A.Y.T.P., I.A., and W.Y.H. contributed equally to this work.

[2]Present address: Department of Life Science, Tunghai University, 407224 Taichung, Taiwan.

[3]To whom correspondence may be addressed. Email: shuochien@gmail.com.

This article contains supporting information online at https://www.pnas.org/lookup/suppl/doi:10.1073/pnas.2007806117/-/DCSupplemental.

First published October 30, 2020.

(PD) animal models (29, 30). Furthermore, chemotherapy-induced cognitive impairment may be caused by the activation of microglia and astrocytes that impact on oligodendrocyte lineage cells (31).

Contributions from nonneuronal cells to neuronal dysfunctions has been documented for AD, ALS, and other neurodegenerative diseases (32). While astrocytes derived from sporadic ALS patients, presumably with TDP-43 pathology, are toxic to motor neurons (33–35), astrocytes expressing ALS-causing mutations in TDP-43 have been reported to either inhibit or have no effect on motor neuron survival (36–39). In addition, sporadic ALS patients show demyelination in the motor cortex and spinal cord and enhanced immunoreactivity for neural/glial antigen 2 (NG2), a marker of oligodendrocyte precursor cells (OPCs) (40). Taken together, these findings suggest that glial dysfunction may contribute TDP-43–mediated toxicity.

To address the normal physiological function of TDP-43 in different glia populations and determine how TDP-43–mediated glial dysfunction contributes to neurodegeneration, we and others have inactivated TDP-43 in oligodendrocytes and microglia in mice (41, 42). We demonstrated that TDP-43 is required for oligodendrocyte survival and myelination by regulating the expression of myelin-related genes, and that loss of oligodendroglial TDP-43 expression leads to progressive neurological phenotypes and early lethality (41), whereas, Paolicelli et al. (42) showed that TDP-43 is required for microglial phagocytosis and microglial TDP-43 deletion results in loss of synapses. In this study, we selectively deleted TDP-43 in astrocytes and found that TDP-43–deleted astrocytes acquire a molecular signature resembling A1-reactive astrocytes. These TDP-43–deleted astrocytes affect the function of microglia as well as the survival of mature oligodendrocytes. Taken together, our results suggest both cell-autonomous (astrocytes, where TDP-43 is deleted) and noncell-autonomous (microglia and oligodendrocytes, where TDP-43 appears to localize normally in the nucleus) effects due to TDP-43 loss in astrocytes.

Results

Astrocytic TDP-43 Depletion Results in Cell-Autonomously Larger Astrocytic Territories. In order to investigate the normal physiological function of TDP-43 in astrocytes, and how loss of astroglial TDP-43 may contribute to ALS, conditional TDP-43 (*Tardbp*$^{fl/fl}$) mice were crossed with the glial fibrillary acidic protein (GFAP)-Cre mouse line, in which the Cre-recombinase expression is driven by the human GFAP promoter (43) (hereafter referred to as *GFAP*-Cre). We first evaluated the cell-type–specificity of Cre-mediated recombination by breeding *GFAP*-Cre mice with *Rosa26*-GFP-NLS-LacZ (GNZ) (hereafter referred to as *Rosa*-GNZ) reporter mice (*SI Appendix*, Fig. S1*A*), where the ubiquitously expressing *Rosa26* locus contains a *loxP*-STOP-*loxP* cassette preceding a GNZ fusion protein (44). To determine the exact cell type in which Cre-mediated recombination occurs, double labeling with GFP and specific cell markers was conducted. Over 90% of the cells positive for GFAP expression were also positive for GFP (90.6 ± 1.0%) (*SI Appendix*, Fig. S1 *B* and *C*), in contrast to very little colocalization of GFP with the neuronal marker NeuN (1.8 ± 0.6%) (*SI Appendix*, Fig. S1 *B* and *D*) or Olig2^{+} oligodendrocyte lineage cells (12.6 ± 0.7%) (*SI Appendix*, Fig. S1 *B* and *E*). Because GFAP-Cre appears to be active in ∼10% of Olig2^{+} cells, we further investigated the potential excision in oligodendrocyte lineage cells using Sox10 (labels oligodendrocyte lineage cells), NG2 (labels OPCs), and APC-CC1 (labels mature oligodendrocytes) antibodies (*SI Appendix*, Fig. S2 *A–C*), revealing 2.1 ± 1.8% of Sox10/GFP–, 9.8 ± 5.8% of NG2/GFP–, and 0.3 ± 0.9% of APC-CC1/GFP–double-positive cells (*SI Appendix*, Fig. S2 *A–C*). Finally, we found very little overlap between GFP and Iba1 (microglia marker) expression (3.1 ± 4.2%). These results indicate that *GFAP*-Cre–mediated recombination in the spinal cord is largely restricted to astrocytes.

We next bred *Tardbp*$^{fl/fl}$ mice with *GFAP*-Cre mice to selectively delete TDP-43 in astrocytes. The resulting offspring followed the expected Mendelian ratio for the possible genotypes: *Tardbp*$^{fl/+}$, *Tardbp*$^{fl/fl}$, *GFAP-Cre;Tardbp*$^{fl/+}$, and *GFAP-Cre;Tardbp*$^{fl/fl}$ (Fig. 1*A*). The specificity of TDP-43 deletion in astrocytes was confirmed by colabeling GFAP and TDP-43 with GFAP^{+} cells devoid of TDP-43 in *GFAP-Cre;Tardbp*$^{fl/fl}$ (abbreviated as "cKO"), but not *Tardbp*$^{fl/fl}$ (abbreviated as "ctr"), and *GFAP-Cre;Tardbp*$^{fl/+}$ (abbreviated as "cHet"), mice (*SI Appendix*, Fig. S3). Due to documented autoregulatory mechanisms (45, 46), the expression level of TDP-43 in the astrocytes of *GFAP*-Cre;*Tardbp*$^{fl/+}$ mice was presumed to be the same as in *Tardbp*$^{fl/fl}$ animals. Indeed, *GFAP*-Cre;*Tardbp*$^{fl/+}$ mice are indistinguishable from *Tardbp*$^{fl/fl}$ mice (see below), both of which were used as controls in the subsequent analyses.

To better quantify the excision efficiency and specificity of TDP-43 loss in astrocytes, spinal cords were divided into dorsal and ventral regions based on the position of the central canal. Astrocytes were identified using a combination of cytoskeletal (GFAP) and nuclear (Sox9) markers. Loss of TDP-43 in GFAP/Sox9–double-positive cells was readily and unambiguously identified (Fig. 1*B* and *SI Appendix*, Fig. S2). Quantitative analyses revealed that 90.9 ± 4.1% and 63.2 ± 6.8% of astrocytes harbored TDP-43 deletion within the dorsal and ventral gray matter of *GFAP-Cre;Tardbp*$^{fl/fl}$ mice, respectively (Fig. 1*C*). This indicates that TDP-43 is deleted in a specific, but nonuniform fashion within the mouse spinal cord.

We next sought to biochemically determine the extent of TDP-43 deletion in astrocytes. To this end, we first quantified TDP-43 expression in astrocytes and oligodendrocytes. Astrocytes and oligodendrocytes were isolated from the wild-type mouse cerebral cortex using the cell surface markers, ACSA-2 and O4, respectively (Fig. 1*D*). The purity of astrocytes and oligodendrocytes were confirmed with GFAP or ALDH1L1 (astrocyte markers) and myelin basic protein (MBP, myelinating oligodendrocyte marker), whereas PSD-95 (neuron marker) was diminished in the astrocyte and oligodendrocyte fractions (Fig. 1*D*). Using a known amount of recombinant mouse TDP-43, TDP-43 expression was estimated to be four times higher in astrocytes relative to oligodendrocytes (8 ng and 2 ng of TDP-43 in 20 μg of astrocyte and oligodendrocyte lysates, respectively) by immunoblotting (Fig. 1*D*). To estimate the extent of TDP-43 deletion in astrocytes, spinal cords from *Tardbp*$^{fl/fl}$ and *GFAP-Cre;Tardbp*$^{fl/fl}$ mice were used. Astrocytes and oligodendrocytes were isolated by FACS (Fig. 1*E*). The enrichment of astrocytes and oligodendrocytes was confirmed by qRT-PCR of *Aldh1l1* and *Cnp* genes (Fig. 1*E*), revealing a 50% reduction in TDP-43 expression in the astrocyte fractions (Fig. 1*E*).

When TDP-43 was reduced in astrocytes, GFAP immunoreactivity appear to be increased (Fig. 1*B*, arrow) relative to astrocytes with TDP-43 expression (Fig. 1*B*, arrowheads). To better quantify astrocytic morphological changes, individual astrocytes were traced based on GFAP staining from the dorsal and ventral horn of *Tardbp*$^{fl/fl}$, *GFAP-Cre;Tardbp*$^{fl/+}$, and *GFAP-Cre;Tardbp*$^{fl/fl}$ mice. The astrocytes in the *GFAP-Cre;Tardbp*$^{fl/fl}$ mice were further classified based on the presence (TDP-43^{+}) or absence (TDP-43^{-}) of TDP-43 expression (Fig. 2*A*). Astrocytes with TDP-43 deletion showed a twofold increase in total process length and number compared to astrocytes with TDP-43 expression (Fig. 2 *B* and *C*). The magnitude of change was similar between dorsal and ventral parts of the spinal cord (dorsal process length: 1.9-fold, $P < 0.01$; ventral process length, 2.3-fold, $P < 0.001$; dorsal process numbers: 2.1-fold, $P < 0.001$; ventral process numbers, 2.3-fold, $P < 0.001$). Furthermore, the total length of the processes and the number of processes in astrocytes with TDP-43 were comparable in *Tardbp*$^{fl/fl}$, *GFAP-Cre;Tardbp*$^{fl/+}$, and *GFAP-Cre;Tardbp*$^{fl/fl}$ mice (Fig. 2 *B* and *C*), suggesting that astrocytes without TDP-43 expression exhibit cell-autonomous morphological changes.

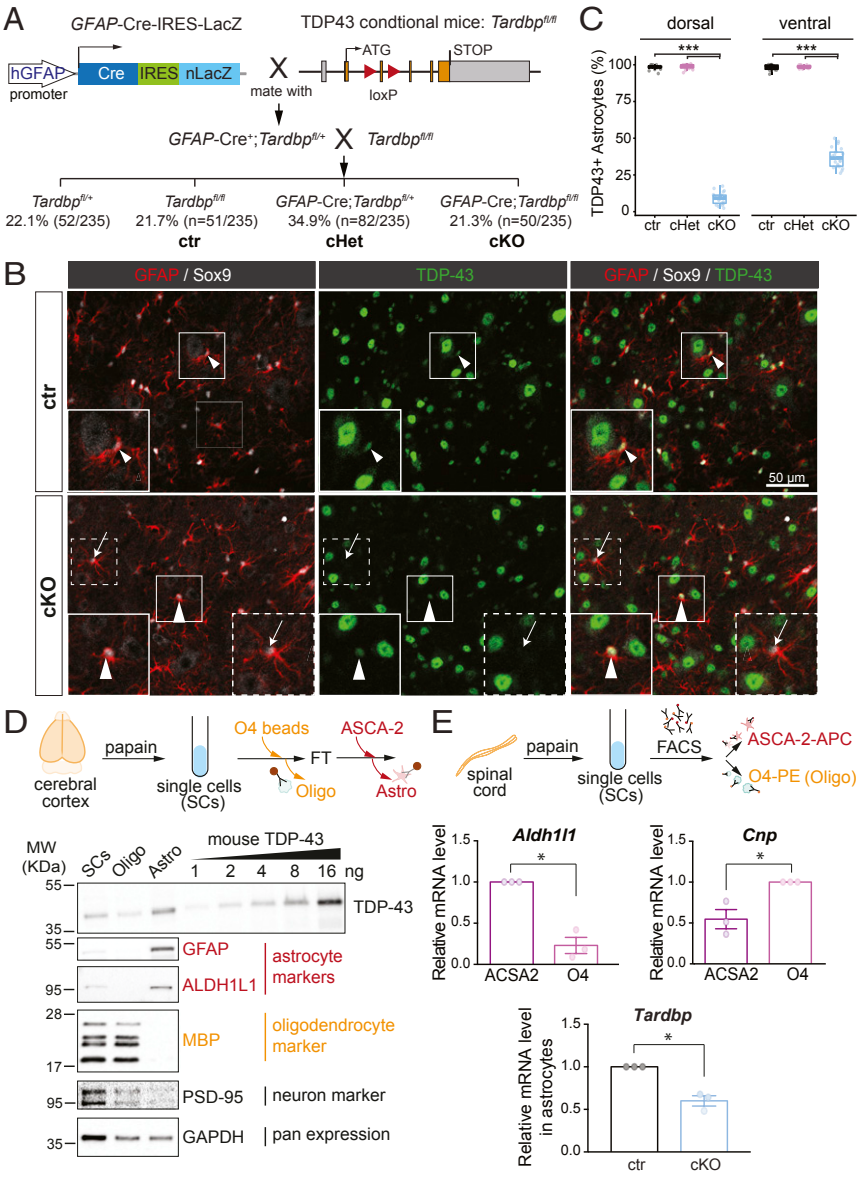

Fig. 1. TDP-43–deleted astrocytes have enhanced GFAP immunoreactivity. (*A*) Mating strategy to generate *GFAP-Cre;Tardbp*$^{fl/fl}$ mice. The resultant mice genotypes, *Tardbp*$^{fl/+}$, *Tardbp*$^{fl/fl}$ (ctr), *GFAP-Cre;Tardbp*$^{fl/+}$ (cHet), *GFAPCre;Tardbp*$^{fl/fl}$ (cKO) were in expected Mendelian ratio of 1:1:1:1, with a cohort of 235 live pups yielding 22.1% *Tardbp*$^{fl/+}$, 21.7% ctr, 34.9% cHet, and 21.3% cKO mice. (*B*) Confocal images of spinal cord sections colabeled with TDP-43 (green) and astrocyte markers [GFAP (red) and Sox9 (gray)] in ctr and cKO mice. GFAP/Sox9–double-positive astrocytes without TDP-43 (arrow) show enhanced GFAP immunoreactivity compared to GFAP/Sox9–double-positive astrocytes with TDP-43 (arrowhead). (Enlargement, 2× zoom.) (Scale bar, 50 µm.) (*C*) Excision efficiency and specificity across the dorsal (*Left*) and ventral (*Right*) gray matter of spinal cords of ctr, cHet, and cKO mice. Significant loss of TDP-43 expression in cKO mice, with dorsal and ventral differences in efficiency observed (***$P < 0.001$, $n = 3$ for each genotype, $n > 6$ sections per mouse). (*D*, *Upper*) Schematic for isolation of oligodendrocytes and astrocytes using O4 and ACSA-2 magnetic beads from the mouse cerebral cortex. (*Lower*) Immunoblots for TDP-43, GFAP, ALDH1L1, MBP, PSD-95, and GAPDH expression. Astro: astrocyte fraction; FT: flow through; Oligo: oligodendrocyte fraction; SCs: single cells fractions, (*E*, *Upper*) Schematic for the isolation of oligodendrocytes and astrocytes from the mouse spinal cord using FACS. qRT-PCR for *Aldh1l1* and *Cnp* in astrocytes and oligodendrocytes fractions confirm the enrichment of each cell type. mRNA expression of *Tardbp* (TDP-43) is reduced in astrocytes cKO mice. $n = 3$, *$P < 0.05$.

Astrocytic TDP-43 Depletion Induces A1-Like Reactive Astrocytes. To define the molecular changes associated with TDP-43 loss in astrocytes, RNA sequencing (RNA-seq) of whole spinal cords of 3-mo-old *Tardbp*$^{fl/fl}$, *GFAP-Cre;Tardbp*$^{fl/+}$, and *GFAP-Cre;Tardbp*$^{fl/fl}$ mice was performed. Principal component analysis revealed that *GFAP-Cre;Tardbp*$^{fl/fl}$ samples cluster separately from *Tardbp*$^{fl/fl}$ and *GFAP-Cre;Tardbp*$^{fl/+}$ samples, which cluster together (*SI Appendix*, Fig. S4*A*). Pairwise comparisons revealed that the global gene-expression patterns in *GFAP-Cre;Tardbp*$^{fl/fl}$ mice were distinct from *Tardbp*$^{fl/fl}$ and *GFAP-Cre;Tardbp*$^{fl/+}$ mice (*SI Appendix*, Fig.S4 *B–D*). Differential gene-expression analysis contrasting *GFAP-Cre;Tardbp*$^{fl/fl}$ with *Tardbp*$^{fl/fl}$ yielded 624 significantly dysregulated genes (427 up and 197 down differentially expressed genes [DEGs]) (Fig. 3*A*). Comparisons between *Tardbp*$^{fl/fl}$ and *GFAP-Cre;Tardbp*$^{fl/+}$ samples yielded only 29 DEGs, suggesting that they were nearly indistinguishable (*SI Appendix*, Fig. S4*B*). Further downstream analysis focused on comparisons between *GFAP-Cre;Tardbp*$^{fl/fl}$ and *Tardbp*$^{fl/fl}$ samples.

Gene ontology (GO) terms revealed functional divergences in the enriched up- and down-regulated GO terms (Fig. 3*B*). The top five up-regulated GO terms were associated with energy and metabolic processes, including nucleoside monophosphate metabolic process, monovalent inorganic cation transport, and cofactor metabolic factors. The top five down-regulated GO terms included ensheathment of neurons (with associated down-regulation of myelination genes, such as *Mag*, *Myrf*, and *Plp1*), gliogenesis, axon development, regulation of transsynaptic signaling, and negative-regulation of cell projection. Although the down-regulated GO terms are functionally distinct, these GO groups appear to reflect reactive astrocytosis (28, 47).

To further elucidate astrocyte changes in the TDP-43–deleted astrocytes, we performed gene set enrichment analysis (GSEA) using known transcriptomic signatures of pan-reactive astrocytes, including A1 and A2 astrocytes (28, 47) (Fig. 3*C*). The proposed or known functions of these pan-reactive A1 and A2 astrocyte markers are listed in the *SI Appendix*, Table S1. The A1-specific signature and the pan-reactive astrocyte signature were significantly and positively enriched (Fig. 3*D*), suggesting an A1-like molecular profile in TDP-43–deleted astrocytes. qRT-PCR assays confirmed the increased expression of the pan-reactive marker, *Serpina3n* (Fig. 3*E*), and A1-reactive markers, *C3* and *Ligp1* (Fig. 3 *F* and *G*). The up-regulated genes appear to participate in a complement system and activity (such as *C3* and *Serping1*) and be part of class I major histocompatibility complex (MHC) molecules

(such as *H2-D1* and *H2-T23*) (*SI Appendix*, Table S1). In contrast, there was no apparent up-regulation of the astrocyte-enriched gene set (23) (*SI Appendix*, Fig. S5). Collectively, these data suggest that TDP-43–deleted astrocytes harbor an A1-like reactive signature.

Astrocytic TDP-43 Depletion Does Not Increase Astrocyte or Microglia Proliferation, but Induces C1q Expression. A1-reactive astrocytes were originally described as being activated by reactive microglia that release IL-1α, TNF, and C1q (28). To investigate microglia activation in the spinal cords of mice with astroglial TDP-43 deletion, we examined Iba1 expression by immunofluorescence. No change in the Iba1 staining pattern or intensity was observed in *Tardbp*$^{fl/fl}$, *GFAP-Cre;Tardbp*$^{fl/+}$, and *GFAP-Cre;Tardbp*$^{fl/fl}$ mice (Fig. 4*A*). Since the RNA-seq analysis revealed that component factor 1q (*C1qa*, *C1qb*, *C1qc*) was uniquely up-regulated in *GFAP-Cre;Tardbp*$^{fl/fl}$ mice (Fig. 4*B*, *Top*), we confirmed increased *C1qa* and *C1qb* expression by qRT-PCR (Fig. 4*C*). No discernable changes were found in the proinflammatory and anti-inflammatory genes among all three genotypes (Fig. 4*B*, *Middle* and *Bottom*) (28, 48–51).

Enhanced GFAP-immunoreactivity and the presence of an A1-like molecular signature suggests a possible astrogliosis phenotype, which is characterized with astrocyte proliferation (52). We next quantified the numbers of astrocytes using double-labeling of GFAP and Sox9 in both dorsal and ventral gray matters of the spinal cords. Quantification of GFAP/Sox9–double-positive astrocytes showed that the numbers of astrocytes were comparable across the different genotypes (Fig. 4*D*). To analyze astrocyte and microglia proliferation, 5-ethynyl-2′deoxyuridine (EdU) was injected for 2 consecutive days followed by 5 d of chase starting at postnatal day 90 (P90). The number of newly proliferating astrocytes and microglia were quantified by EdU costaining with astrocyte (Sox9) and microglia (Iba1) markers (Fig. 4*E*). No difference in the total numbers of EdU$^+$ cells was found among genotypes (Fig. 4*F*). Furthermore, quantification of the number of EdU/Sox9–double-positive astrocytes (Fig. 4*H*) and EdU/Iba1–double-positive microglia (Fig. 4*G* and *SI Appendix*, Fig. S6) showed comparable numbers across three different genotypes, establishing no change in astrocyte or microglia proliferation. In addition, we found very low and comparable TDP-43 immunofluorescence signals in Iba1$^+$ microglia across the three genotypes (*SI Appendix*, Fig. S7). Taken together, these data suggest that TDP-43–deleted astrocytes 1) cell-autonomously acquire the molecular signature of A1-like reactive astrocytes without affecting astrocyte and microglia proliferation, and 2) non-cell-autonomously induce microglia to increase their expression of components of the C1 complement system.

Astrocytic TDP-43 Depletion Does Not Induce Motor Neuron Degeneration. A1 astrocytes have been shown to affect the survival and function of neurons and oligodendrocytes (28). We next sought to determine whether spinal cord motor neurons were susceptible to TDP-43 loss in astrocytes using choline acetyltransferase (ChAT) antibodies to label spinal cord motor neurons (Fig. 5*A*). There was no significant difference in the number of motor neurons across the genotypes (Fig. 5*B*). However, there were ∼10% ChAT$^+$ motor neurons (9.4 ± 13.8%) that showed loss of TDP-43 expression in *GFAP-Cre;Tardbp*$^{fl/fl}$ mice (Fig. 5*C*). The data suggest that loss of astroglial TDP-43 does not cause motor neuron degeneration.

As denervation at the neuromuscular junction (NMJ) has been proposed to be an early event in the development of ALS, we next investigated the degree of innervation by quantifying the NMJs within the gastrocnemius muscle. Muscle sections were costained with presynaptic neuronal markers, synaptophysin and neurofilament, and fluorescence-tagged α-bungarotoxin, which labels postsynaptic muscular acetylcholine receptors (Fig. 5*D*). Innervation across all genotypes was found to be indistinguishable with 100% intact NMJs (Fig. 5*E*). Furthermore, we also quantified the areas of NMJs and found no difference across the three genotypes (Fig. 5*F*), demonstrating that astroglial deletion of TDP-43 does not lead to NMJ denervation.

Astrocytic TDP-43 Depletion Reduces Mature Oligodendrocytes. GO enrichment analysis showed a down-regulation of "ensheathment of neurons" (Fig. 3*B*), suggesting that myelinating oligodendrocytes may be affected in the spinal cords of astroglial TDP-43–deleted mice. To test this possibility, we computationally estimated the cell type composition using the dampened weighted least-squares (DWLS) algorithm (53). Cell-type signatures were first derived from brain single-cell RNA-seq data from the Mouse Cell Atlas (53, 54), and subsequently used to "deconvolute" the

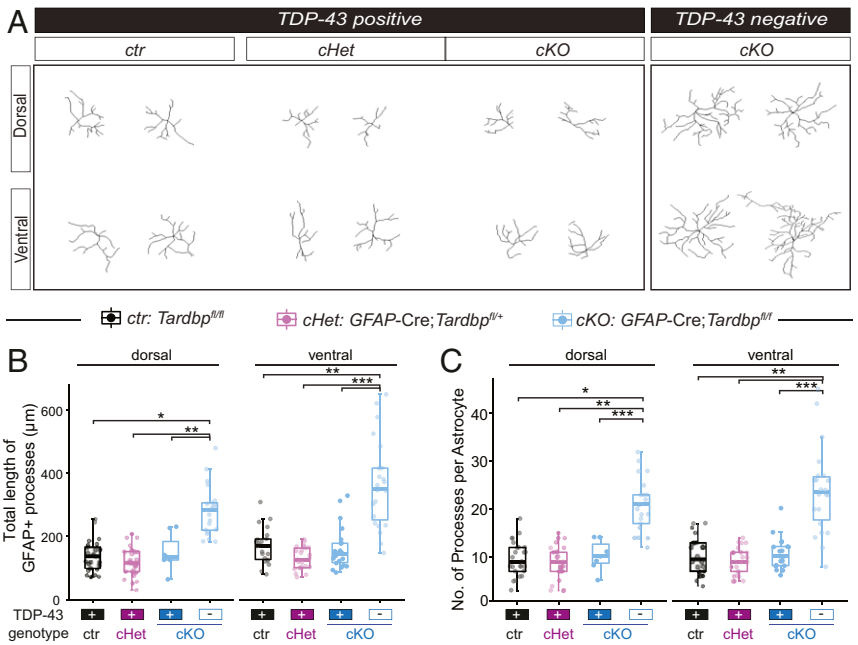

Fig. 2. TDP-43–deleted astrocytes exhibit enhanced GFAP immunoreactivity. (*A*) Representative images of GFAP tracing of astrocytes within the dorsal (*Upper* row) and ventral (*Lower* row) gray matter of spinal cords from *Tardbp*$^{fl/fl}$ (ctr), *GFAP-Cre;Tardbp*$^{fl/+}$ (cHet), *GFAP-Cre;Tardbp*$^{fl/fl}$ (cKO) mice. TDP-43$^+$ and TDP-43$^-$ denotes astrocytes with and without TDP-43, respectively. (*B*) Quantification of total process length of GFAP$^+$ astrocytes within the dorsal (*Left*) and ventral (*Right*) gray matter of spinal cords from ctr, cHet, and cKO mice. At least three sections per animal, three animals per genotype, and three to six astrocytes per region (dorsal/ventral) were traced. (*C*) Quantification of the number of processes of GFAP$^+$ astrocytes within the dorsal (*Left*) and ventral (*Right*) gray matter of spinal cords from ctr, cHet, and cKO mice. At least three sections per animal, three animals per genotype, and three to six astrocytes per region (dorsal/ventral) were traced. $*P < 0.05$, $**P < 0.01$, $***P < 0.001$.

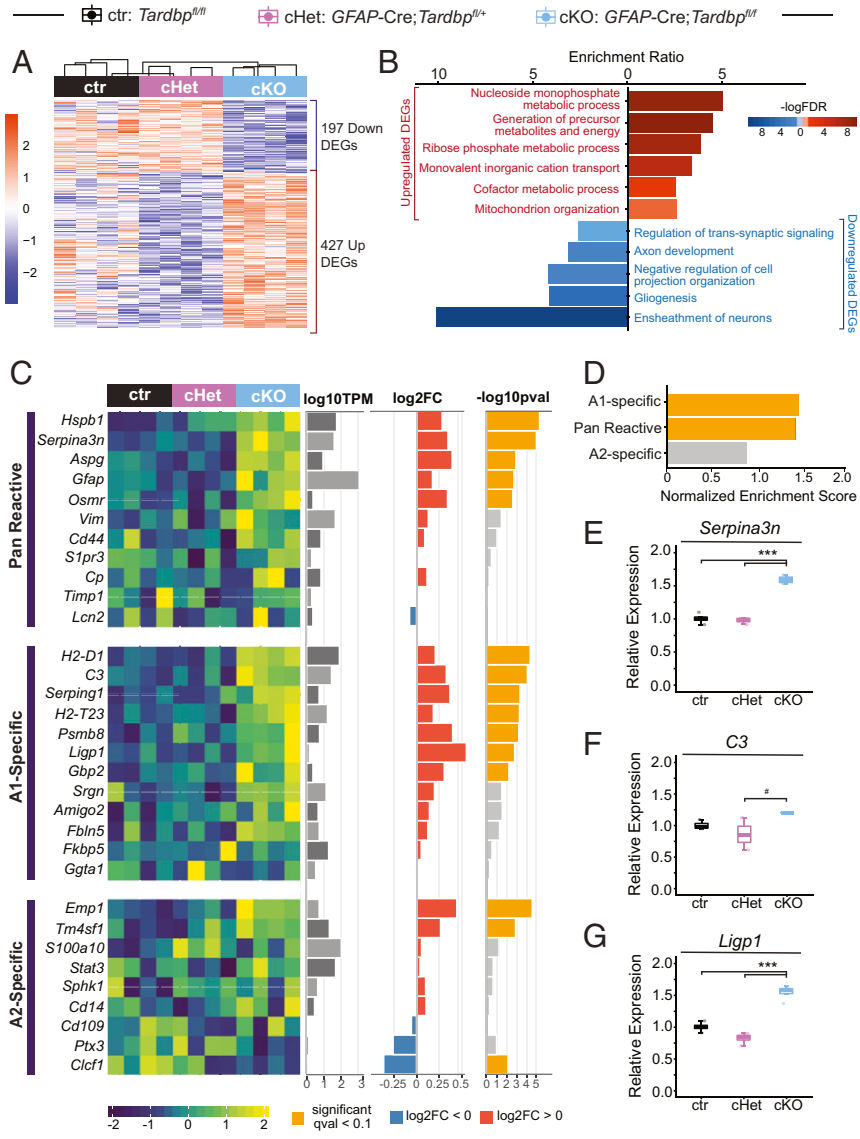

Fig. 3. TDP-43–deleted astrocytes exhibit molecular signatures of A1-reactive astrocytes. (*A*) Hierarchical clustering of the RNA-seq count data clusters *GFAP-Cre;Tardbp*$^{fl/fl}$ (cKO) samples separately from *Tardbp*$^{fl/fl}$ (ctr), *GFAP-Cre;Tardbp*$^{fl/+}$ (cHet) samples, revealing a distinct transcriptome profile. (*B*) The top overrepresented GO (Biological Process) terms in the up- and down-regulated differentially expressed genes in cKO samples as compared to ctr samples. (*C*) Heat map of the expression level of the signature genes for the pan-reactive, A1 and A2 astrocytes in ctr, cHet, and cKO samples, along with their mean expression levels (log10TPM), and the fold-change (log2FC) and *P* value (-log10*p*val) of cKO samples compared to ctr samples. Positive and negative fold-changes are colored in red and blue, respectively, and *P* values corresponding to significant *q*-values (<0.1) are colored in yellow. (*D*) GSEA of pan-reactive, A1 and A2 astrocyte transcriptomic signatures for cKO samples versus ctr and cHET samples. Significantly enriched A1 astrocyte and pan-reactive astrocyte signatures are colored in yellow. (*E*–*G*) Relative mRNA expression for the pan-reactive astrocyte marker, Serpina3n (*E*), and A1-reactive astrocyte markers, C3 (*F*) and Ligp1 (*G*), from the spinal cords of ctr, cHet, cKO mice at P90, as quantified by qRT-PCR. *Serpina3n, C3* and *Ligp* expression were elevated in cKO mice. $^{\#}P < 0.1$, $^{***}P < 0.001$, $n = 4$ per genotype.

bulk RNA-seq data (Fig. 6*A*). The computational model predicts a significant reduction of the proportion of mature myelinating oligodendrocytes, but not OPCs (Fig. 6*A*). Indeed, analysis of the myelin structural genes (Fig. 6 *B*, *Top*) and the oligodendrocyte-enriched genes (23) (Fig. 6 *B*, *Middle*) revealed consistently reduced expression in the *GFAP-Cre;Tardbp*$^{fl/fl}$ mice. In contrast, the expression levels of OPC-enriched genes were comparable (Fig. 6 *B*, *Bottom*), suggesting a potential reduction in mature oligodendrocytes, but not OPCs.

To confirm the reduction of mature oligodendrocytes in astroglial TDP-43–deleted mice, we quantified the number of mature oligodendrocytes using a mature oligodendrocyte marker (APC-CC1) (41, 55). CC1^{+} mature oligodendrocytes in *GFAP-Cre;Tardbp*$^{fl/fl}$ mice were reduced to 60% ($P = 0.0439$) and 58% ($P = 0.02$) of wild-type levels in the spinal cord dorsal and ventral gray matter, respectively (Fig. 6*C* and *SI Appendix*, Fig. S8). Although CC1^{+} mature oligodendrocytes were reduced by 22% in the white matter, this trend did not reach statistical significance ($P = 0.236$) (Fig. 6*C*). In contrast, quantification of NG2^{+} OPCs revealed comparable numbers of OPCs in the dorsal and ventral gray matter and white matter in the three genotypes (*SI Appendix*, Fig. S9). Taken together, these data confirm the computational results demonstrating a selective reduction in mature oligodendrocytes without affecting OPCs.

To further evaluate whether there were any changes in the proliferation and differentiation of oligodendrocyte lineage cells, EdU was injected for 2 consecutive days followed by 5 d of chase. The numbers of EdU/NG2–double-positive cells were comparable in the three genotypes (Fig. 6*D* and *SI Appendix*, Fig. S10), demonstrating no change in OPC proliferation. Similarly, the number of EdU/CC1–double-positive cells was comparable between the gray and white matter in the three genotypes (Fig. 6*E*), suggesting normal differentiation of OPCs into mature oligodendrocytes. As ∼10% of GFP^{+} cells labeled with Olig2 (*SI Appendix*, Fig. S1) and NG2 (*SI Appendix*, Fig. S2) in *GFAP-Cre;Rosa*-GNZ mice, and mature oligodendrocytes with TDP-43 depletion exhibit cell-autonomous degeneration (41), it is possible that the loss of mature oligodendrocytes observed in astroglial TDP-43–deleted mice may be due to GFAP-Cre–mediated recombination in oligodendrocyte lineage cells. To address this possibility, we evaluated the extent of potential TDP-43 deletion in oligodendrocyte lineage cells. Because the *GFAP*-Cre transgene contains a LacZ expression cassette (43) (Fig. 1*A*), we examined the costaining pattern of LacZ and Sox10, a highly expressed

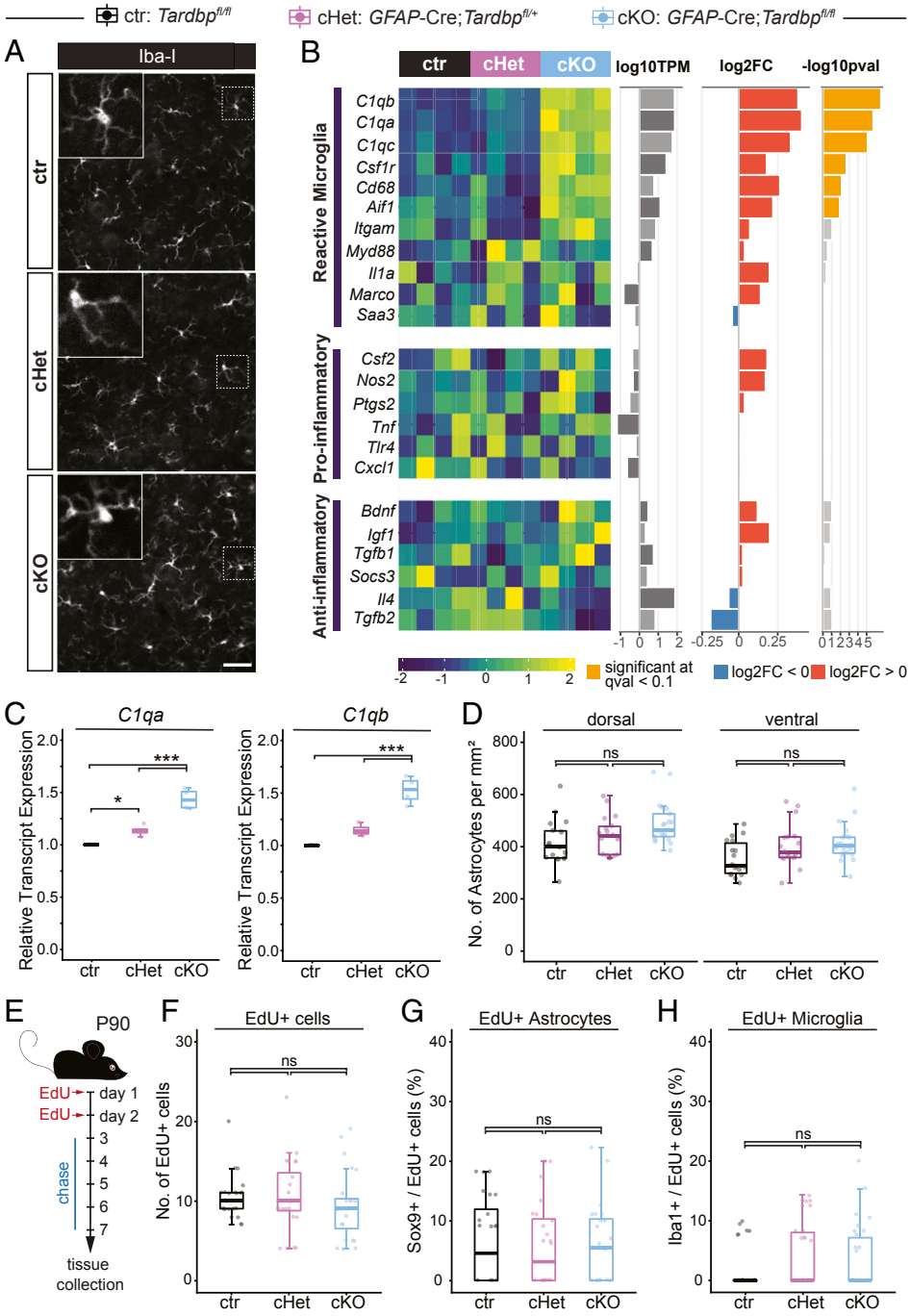

Fig. 4. TDP-43–deleted astrocytes cause increased C1q expression in microglia without changing astrocyte or microglia proliferation. (*A*) Confocal images of the gray matter of lumbar spinal cords from *Tardbp*$^{fl/fl}$ (ctr), *GFAP-Cre;Tardbp*$^{fl/+}$ (cHet), *GFAP-Cre;Tardbp*$^{fl/fl}$ (cKO) mice immunostained with the microglial marker, Iba1. (Enlargement, 3× zoom.) (Scale bar, 50 μm.) (*B*) Heat map of the expression levels of the signature genes for reactive microglia, as well as proinflammatory and antiinflammatory cytokines in ctr, cHet, and cKO samples, along with their mean expression levels (log10TPM), and the fold-change (log2FC) and *P* value (-log10*p*val) of cKO samples relative to ctr samples. (*C*) *C1qa* and *C1qb* relative mRNA expression in the spinal cords of ctr, cHet, and cKO mice at P90 as quantified by qRT-PCR. **P* < 0.05, ****P* < 0.001; ns, not significant. *n* = 4 per genotype. (*D*) Quantification of GFAP/Sox9–double-positive astrocytes in the dorsal and ventral gray matter of lumbar spinal cords from ctr, cHet, and cKO mice. *n* = 3 per genotype, 6–8 sections per animal. ns, not significant. (*E*) Schematic of EdU pulse-chase experiment. ctr, cHet, and cKO mice were injected with EdU for 2 consecutive days followed by a 5 d of chase before tissue collection. (*F*) Quantification of EdU^{+} cells in the gray and white matter of the lumbar spinal cord. *n* = 3 per genotype, 6–10 sections per animal. ns, not significant. (*G*) Quantification of EdU/Sox9–double-positive astrocytes in the dorsal and ventral gray matter of the lumbar spinal cords from ctr, cHet, and CKO mice. *n* = 3 per genotype, 6–10 sections per animal. ns, not significant. (*H*) Quantification of EdU/Iba1–double-positive microglia in the dorsal and ventral gray matter of the lumbar spinal cords from ctr, cHet, and cKO mice. *n* = 3 per genotype, 6–10 sections per animal were analyzed. ns, not significant.

transcription factor that is restricted to oligodendrocyte lineage cells within the CNS (23, 56), of *GFAP-Cre;Tardbp*$^{fl/+}$ mice. LacZ and Sox10 labeled distinct populations of cells in both the gray and white matter (*SI Appendix*, Fig. S11), revealing that Cre recombinase is not expressed in oligodendrocyte lineage cells at 3 mo of age. Furthermore, we quantified the expression of TDP-43 in CC1^{+}, NG2^{+}, or Sox10^{+} cells. The quantification showed comparable percentages of TDP-43/CC1–, TDP-43/NG2–, and

TDP-43/Sox10–double-positive cells in all three genotypes (Fig. 6*F* and *SI Appendix*, Fig. S12). Finally, we examined TDP-43 expression in isolated oligodendrocytes from *Tardbp*$^{fl/fl}$ and *GFAP-Cre;Tardbp*$^{fl/fl}$ mice using the O4 surface marker. No changes were observed for the *Tardbp* mRNA and TDP-43 protein expression in isolated oligodendrocytes from *GFAP-Cre;Tardbp*$^{fl/fl}$ mice (Fig. 6 *G* and *H*). Taken together, these data indicate that TDP-43 is not depleted in oligodendrocyte lineage cells of the *GFAP-Cre;Tardbp*$^{fl/fl}$ mice.

Nevertheless, it is possible that TDP-43 deletion in the oligodendrocyte lineage cells occurs early in the development of the *GFAP-Cre;Tardbp*$^{fl/fl}$ mice. To address this possibility, RNA-seq was performed on the whole spinal cords from *Tardbp*$^{fl/fl}$ *CNP-Cre;Tardbp*$^{fl/+}$(CNP-cHet), and *CNP-Cre;Tardbp*$^{fl/fl}$ (CNP-cKO) mice at P21 (presymptomatic stage) and P60 (end-stage), as previously described (41). GSEA of CNP-cKO mouse samples relative to their respective controls showed an early and progressive positive enrichment of transcriptional signatures of both reactive astrocytes and activated microglia at P21 and P60, which was distinct from that observed following astroglial TDP-43 deletion (*SI Appendix*, Fig. S13; details of the transcriptional signatures provided in *SI Appendix*, Fig. S14). The CNP-cKO mouse samples showed positive enrichment of both A1-specific and A2-specific reactive astrocyte markers at P21 and P60, with nearly all of the genes in the gene sets being highly up-regulated, unlike the GFAP-cKO mice, which showed enrichment of only the A1-specific astrocyte gene set. The reactive microglia signature was positively enriched in samples from CNP-cKO mice, with up-regulation of *C1q*, *Tnf*, and *Il1a* genes, suggesting activated microglia in the oligodendrocyte TDP43-deleted mice, which was not seen in astroglial TDP-43–deleted mice. Although, oligodendrocyte numbers were estimated to be reduced in both glial cell TDP-43–deleted mice (with a greater reduction in CNP-cKO mice), CNP-cKO mice are also predicted to have increased OPCs at P60, which was not observed in astroglial TDP-43–deleted mice. These estimates corroborate with the CNP-cKO mice phenotype described previously (41). Additionally, the myelin structure, mature oligodendrocyte, and OPC-enriched transcriptional signatures in the two glial TDP-43–deleted mice genotypes were different (*SI Appendix*, Fig. S15*B*). Taken together, these data indicate that although deletion of TDP-43 in oligodendrocytes and astrocytes result in reduced mature oligodendrocytes, the mechanisms leading to this outcome are different in the two glial cell-type deletions.

Mice with Astrocytic TDP-43 Deletion Develop Motor, but Not Sensory, Deficits. Given the triglial dysfunction in mice with astrocytic TDP-43 deletion, we next sought to determine whether these astroglial TDP-43–deleted mice develop motor and sensory abnormalities.

Although *GFAP-Cre;Tardbp*$^{fl/fl}$ mice develop normally, the body weights of these mice are ∼12% lighter relative to *Tardbp*$^{fl/fl}$ (P = 0.039), and *GFAP-Cre;Tardbp*$^{fl/+}$ (P = 0.0009) mice, respectively (Fig. 7*A*). The general locomotor activity analysis, as assessed by the total distance traveled in the open field, revealed that *GFAP-Cre;Tardbp*$^{fl/fl}$ mice move less (P < 0.001) (Fig. 7*B*). Next, we assessed the motor learning, balance, and coordination

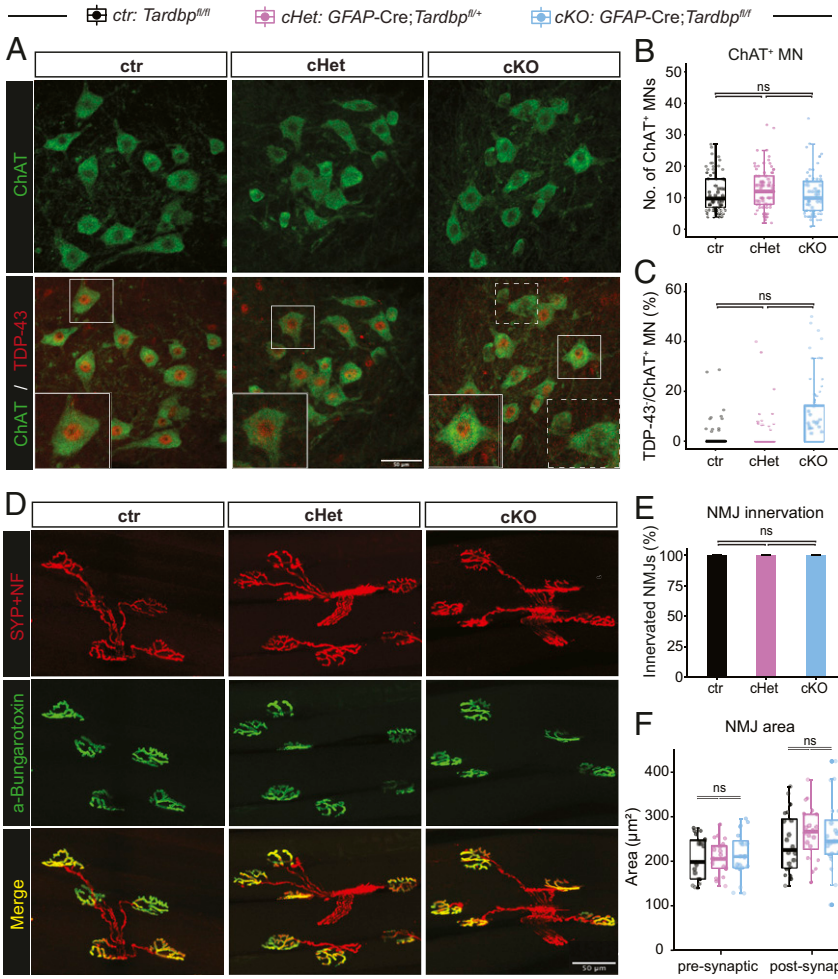

Fig. 5. Astrocyte deletion of TDP-43 does not cause degeneration of motor neurons nor the denervation of NMJs. (*A*) Images through the *z* axis of confocal images of ventral spinal cords of *Tardbp*$^{fl/fl}$ (ctr), *GFAP-Cre;Tardbp*$^{fl/+}$ (cHet), *GFAP-Cre;Tardbp*$^{fl/fl}$ (cKO) mice. The lumbar spinal cord sections were colabeled with ChAT (green) and TDP-43 (red). (Enlargement, 2× zoom.) (Scale bar, 50 μm.) (*B*) Quantification of ChAT$^+$ motor neurons in the ventral horn of the lumbar spinal cord. n = 3 per genotype, at least 8 slices per animal were analyzed. ns, not significant. (*C*) Quantification of ChAT$^+$ and TDP-43$^-$ (ChAT$^+$/TDP-43$^-$) cells in the ventral horn of the lumbar spinal cord. ns, not significant. (*D*) Images through the *z* axis of confocal images of the NMJ from gastrocnemius muscle sections of ctr, cHet, and cKO mice. The muscle sections were colabeled with presynaptic markers: Synaptophysin (red) and neurofilament (red), and postsynaptic marker α-bungarotoxin (green). (Scale bar, 50 μm.) (*E*) Quantification of the innervation status of NMJs using the juxtaposition of pre and postsynaptic markers. n = 3 per genotype, at least 6 slices per animal were analyzed. ns, not significant. (*F*) Quantification of presynaptic and postsynaptic areas labeled by synaptophysin and α-bungarotoxin, respectively. ns, not significant.

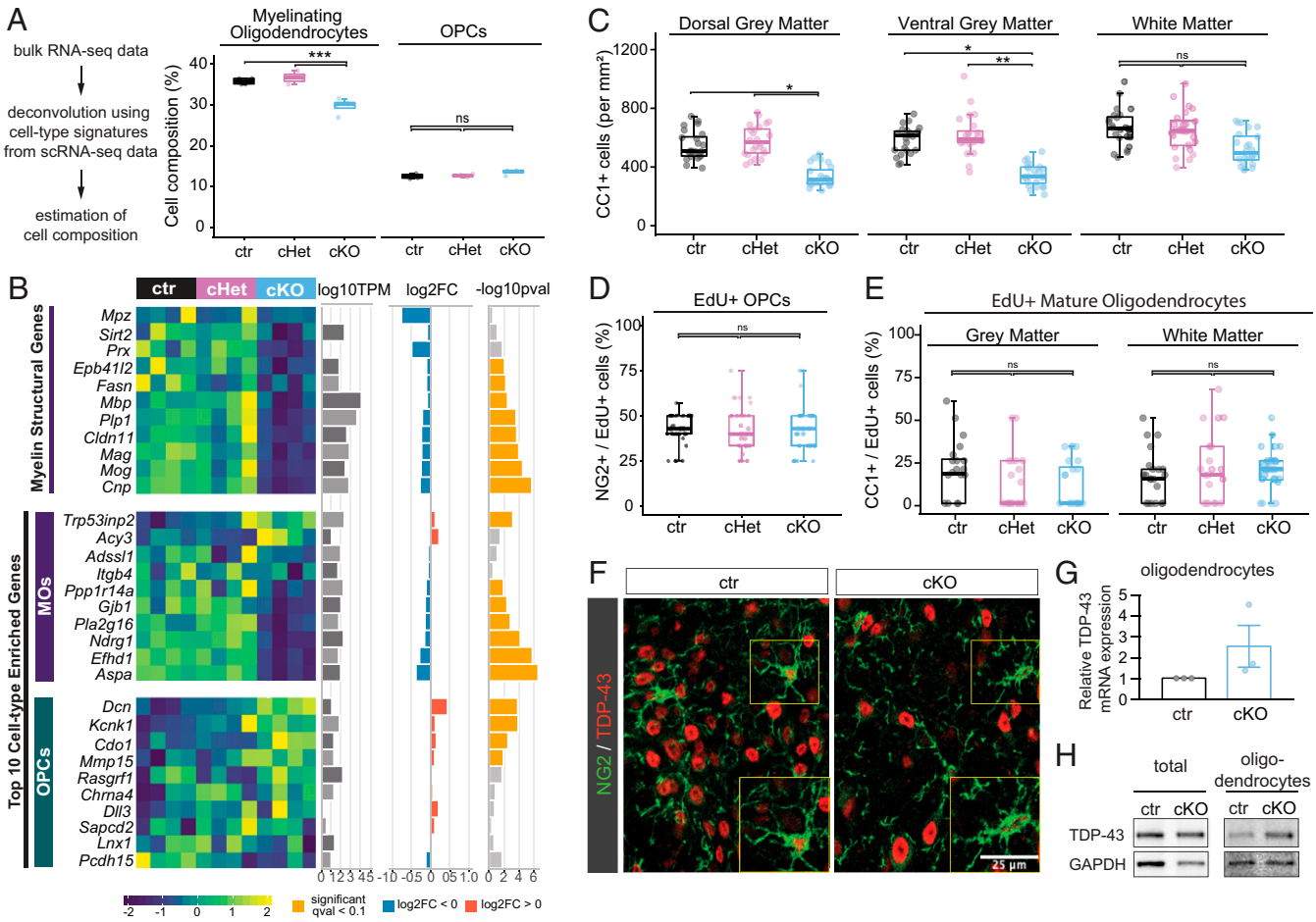

Fig. 6. Reduced mature oligodendrocytes, but not OPCs, in astroglial TDP-43–deleted mice. (*A*) Oligodendrocyte cell composition is estimated to have been reduced in the *GFAP-Cre;Tardbp*$^{fl/fl}$ (cKO) samples as compared to the *Tardbp*$^{fl/fl}$ (ctr), *GFAP-Cre;Tardbp*$^{fl/+}$ (cHet) mice spinal cords. The cell composition was estimated by deconvoluting the bulk RNA-seq data using the DWLS method with cell-type–specific transcriptomic signatures extracted from single-cell RNA-seq data available at the Mouse Cell Atlas v1.1 (54). ***$P < 0.001$. (*B*) Heat map of the expression levels of structural myelin genes. The top cell-type–enriched genes for OPCs and mature oligodendrocytes (MOs) in ctr, cHet, and cKO samples, along with their mean expression levels across all samples (log10TPM), and the fold-change (log2FC) and *P* value (-log10*p*val) of cKO samples compared to ctr samples. Positive and negative fold-changes are colored in red and blue, respectively, and the *P* values corresponding to significant *q*-values < 0.1 are colored in yellow. (*C*) Quantification of CC1$^+$ mature oligodendrocytes in the dorsal gray, ventral gray, and white matter of the lumbar spinal cords from ctr, cHet, cKO mice. $n = 3$ per genotype, at least 8 spinal cord slices per animal were analyzed. *$P < 0.05$, **$P < 0.01$. (*D*) Quantification of EdU/NG2–double-positive astrocytes in the lumbar spinal cords from ctr, cHet, cKO mice. NG2 is used to labeled OPCs. $n = 3$ per genotype, at least 6 spinal cord slices per animal were analyzed. ns, not significant. (*E*) Quantification of EdU/CC1–double-positive astrocytes in the gray and white matter of the lumbar spinal cords from ctr, cHet, cKO mice. $n = 3$ per genotype, at least 6 spinal cord slices per animal were analyzed. ns, not significant. (*F*) Confocal image of gray matter of the lumbar spinal cord of ctr and cKO mice immunostained with NG2, a marker of OPCs (green), and TDP-43. (Scale bar, 25 µm.) (*G*) qRT-PCR for *Tardbp* (TDP-43) in oligodendrocytes isolated from ctr and cKO mice. (*H*) Immunoblots of TDP-43 and GAPDH in single-cell fractions (total) and the oligodendrocyte fraction.

using two different tests: accelerating rotarod and balance beam test. *GFAP-Cre;Tardbp*$^{fl/fl}$ mice could not stay on the accelerating rotarod as long as their age-matched littermate controls ($P < 0.05$) (Fig. 7*C*). During balance beam testing, *GFAP-Cre;Tardbp*$^{fl/fl}$ mice exhibited significantly more paw slips than controls (*Tardbp*$^{fl/fl}$ and *GFAP-Cre;Tardbp*$^{fl/+}$) when walking across the both the 12-mm ($P < 0.05$) and 6-mm beams ($P < 0.01$) (Fig. 7*D*). Finally, grip strength, which measures neuromuscular function, was assessed. *GFAP-Cre;Tardbp*$^{fl/fl}$ mice displayed a reduction in total body grip strength (measuring all four paws) compared to *Tardbp*$^{fl/fl}$ mice ($P = 0.019$) (Fig. 7 *E*, *Right*), but were comparable in forepaw grip strength ($P = 0.713$) (Fig. 7 *E*, *Left*).

To determine whether astroglial TDP-43 deletion affected sensory function, we measured thermal (thermoception) and mechanical sensitivity. In the plantar test for thermal sensitivity, where radiant heat beams were focused on the animal's paw, *GFAP-Cre;Tardbp*$^{fl/fl}$ mice exhibited similar paw-withdrawal latency to controls (Fig. 7*F*). In the dynamic plantar test for mechanical sensitivity, where the animal's paw is subjected to ascending force, GFAP-*Cre;Tardbp*$^{fl/fl}$ mice showed comparable withdrawal times relative to *Tardbp*$^{fl/fl}$ mice, although GFAP-*Cre;Tardbp*$^{fl/+}$ mice showed prolonged paw withdrawal latencies when compared to *Tardbp*$^{fl/fl}$ mice ($P = 0.026$) (Fig. 7 *F*, *Right*). Taken together, mice with astroglial TDP-43 deletion developed deficits in motor, but not sensory, function.

Discussion

In this study, we showed that TDP-43–deleted astrocytes show enhanced GFAP immunoreactivity and acquire a molecular signature resembling A1-like reactive astrocytes. Furthermore, TDP-43–deleted astrocytes induce up-regulation of C1 complement expression in the microglia and reduce the number of mature oligodendrocytes. Although there was no loss of spinal cord motor neurons and no denervation of NMJs, astroglial TDP-43–deletion

mice develop motor deficits, but have intact thermoception and mechanoception. Taken together, these data indicate that TDP-43 is required to maintain astrocytes in a "protective" state (Fig. 8). This triglial dysfunction may underlie the motor deficits observed in astroglial TDP-43–deleted mice. Together with previous efforts in which TDP-43 loss was targeted to mature oligodendrocytes (41) and microglia (42), these findings collectively underscore cell-type–specific functions for TDP-43, and reveal that TDP-43–mediated dysfunction in different cell types contributes to disease pathogenesis through potentially distinct mechanisms.

How astroglial TDP-43 dysfunction contributes to ALS is not clear; however, astrocyte-specific overexpression of the ALS-linked TDP-43 mutant (M337V) protein causes motor neuron degeneration and paralytic phenotypes in rats within 1 mo (36). In contrast, coculture of induced pluripotent stem cell-derived astrocytes harboring the same mutation did not cause motor neuron death in vitro, although M337V-expressing astrocytes have cytoplasmic TDP-43 mislocalization and reduced survival (38). Apparent contradictory results were also obtained using astrocytes cultured from mice expressing another ALS-linked mutation (A315T), which is toxic to rat ventral spinal cord neurons (37), but is not toxic to mouse embryonic stem cell-derived motor neurons (39). It should be noted that astrocytes derived from sporadic ALS patients, presumably with TDP-43 pathology, are toxic to motor neurons, although the source of the toxicity from sporadic ALS astrocytes remains unknown (33–35). On the other hand, transgenic RNAi-based TDP-43 knockdown using a ubiquitous CAG promoter in mice causes ALS-like phenotypes, which Yang et al. (57) suggest is due to TDP-43 reduction in astrocytes, but not motor neurons. In contrast, transplantation of TDP-43–deleted glial-restricted precursor cells did not cause motor neuron degeneration (39). Consistent with this notion, we show that TDP-43 deletion in astrocytes does not cause degeneration of motor neurons nor the denervation at NMJs. Collectively, these data suggest that the loss of astroglial TDP-43 is not sufficient to drive motor neuron degeneration.

Nevertheless, TDP-43–deleted astrocytes exhibit enhanced GFAP immunoreactivity and appear to occupy larger astroglial territories. These morphological changes are cell-autonomous, as the astrocytes retaining TDP-43 expression in *GFAP-Cre;Tardbp*$^{fl/fl}$ mice are similar to astrocytes in *Tardbp*$^{fl/fl}$ and *GFAP-Cre;Tardbp*$^{fl/+}$ mice. At the molecular level, TDP-43–deleted astrocytes acquire an A1-like reactive astrocyte signature (28). It is worth noting that TDP-43–deleted astrocytes do not fully recapitulate A1-reactive astrocytes, as the expression of several A1 genes was not increased in TDP-43–deleted astrocytes. In addition, A1-reactive astrocytes are proposed to be triggered by activated microglia through microglia-derived TNF, IL-1, and C1q production (28). Based on microglial morphology and molecular signatures, microglia in *GFAP-Cre;Tardbp*$^{fl/fl}$ mice do not appear to be activated, although C1q mRNA levels are elevated, suggesting that the A1-like signature of TDP-43–deleted astrocytes is unlikely to result from the activation of microglia, but rather is due to the loss of TDP-43 expression in astrocytes. The absence of a potential feed-forward activation loop involving microglia and astrocytes in *GFAP-Cre;Tardbp*$^{fl/fl}$ mice may explain the lack of a strong gliotic reaction observed.

In contrast, the total numbers of mature oligodendrocytes, but not OPCs, were reduced in *GFAP-Cre;Tardbp*$^{fl/fl}$ mice, without an associated defect in OPC proliferation or differentiation. A1-reactive astrocytes can cause degeneration of mature oligodendrocytes in vitro (28) and in the setting of chemotherapy in vivo (31). In these scenarios, activated microglia induce A1-reactive astrocytes, the latter of which is proposed to cause degeneration of mature oligodendrocytes. Similarly, Li et al. (58) recently showed that astrocytes with GFAP mutations causal for Alexander disease inhibit OPC proliferation and myelination, a disease in which TDP-43 aggregates have been reported (59).

It is possible that TDP-43 is deleted in a small subset of oligodendrocyte lineage cells due to transient *GFAP*-Cre transgene expression in neural progenitor cells during embryonic development (43). To address this possibility, we used five independent approaches. First, using a reporter line (ROSA-GNZ) and a pan-oligodendrocyte marker (Olig2), we estimated that ∼10% of GFP$^+$ cells are also Olig2$^+$. It should be noted that the potential ∼10% excision in oligodendrocytes may be an overestimation, as Olig2 is also expressed in some astrocytes (60). Thus, additional mechanisms likely account for the observed 40% reduction of mature oligodendrocytes in astroglial TDP-43–deleted mice. In addition, the reporter line may not faithfully recapitulate the correct depletion pattern of conditional TDP-43 alleles (61). Second, taking advantage of the LacZ expression cassette within the *GFAP*-Cre transgene, we found that LacZ$^+$ and Sox10$^+$ cells are distinct. As Sox10 is restricted to myelin-forming oligodendrocytes (56), these data suggest that GFAP-Cre is not expressed in the oligodendrocytes at 3 mo of age. Third, the percentage of TDP-43– and Sox10–double-positive oligodendrocyte lineage cells, NG2–double-positive OPCs, or CC1–double-positive mature oligodendrocytes were comparable to controls. Fourth, we do not observe enhanced OPC proliferations, which could be triggered by the degeneration of TDP-43–deleted oligodendrocytes (41), in *GFAP-Cre;Tardbp*$^{fl/fl}$ mice. Finally, no TDP-43 reduction was observed in oligodendrocytes directly isolated from *GFAP-Cre;Tardbp*$^{fl/fl}$ mice.

Taken together, our working model is that TDP-43–deleted astrocytes are toxic to mature oligodendrocytes without affecting OPCs. Furthermore, TDP-43 deletion in both astrocytes and oligodendrocytes is observed to cause change in status of microglia, astrocytes, and oligodendrocytes. In particular, there was pronounced astrocyte and microglia activation proceeding noticeable oligodendrocyte degeneration and demyelination in the oligodendroglial TDP-43–deletion mice. These data further support a close communication between astrocytes, oligodendrocytes, and microglia, and a triglial dysfunction may underlie the neurological phenotypes observed in the astroglial and oligodendroglial TDP-43–deleted mice. Future work using single-cell RNA-seq is planned to address the molecular mechanisms operative in the three types of glia.

Although TDP-43 proteinopathies were originally identified for the majority of ALS and a subgroup of FTD patients (5, 6), recent studies have highlighted the prevalence of TDP-43 pathologies in the brains of old-aged humans (62, 63) and a wide range of neurodegenerative diseases (13), such as AD (64, 65), PD (66), hippocampal sclerosis (67, 68), and limbic-predominant age-related TDP-43 encephalopathy (LATE, a disease with TDP-43 pathology within medial temporal lobe structures in patients over 80 y old) (69). Given that the severity and symptoms of each disease typically corelate with TDP-43 pathology within affected brain regions (63), TDP-43 dysfunction likely contributes to disease onset and progression. Combined with previous studies deleting TDP-43 in mature oligodendrocytes (41) and microglia (42), our findings in astrocytes expand the role of TDP-43–mediated dysfunction in multiple cell types in disease pathogenesis through potentially distinct mechanisms. Delineating the underlying mechanisms would facilitate the development of novel strategies for treating ALS/FTD, AD, and TDP-43–associated proteinopathies-associated diseases and aging.

Materials and Methods

Mouse Models. All studies were carried out under protocols approved by the Institutional Animal Care and Use Committee of the National University of Singapore and were in compliance with Association for Assessment of Laboratory Animal Care guidelines for animal use. All mice used in this study were maintained on a C57BL/6J background and were housed in groups in individually ventilated cages under a 12:12-h light/dark cycle with access to food and water ad libitum.

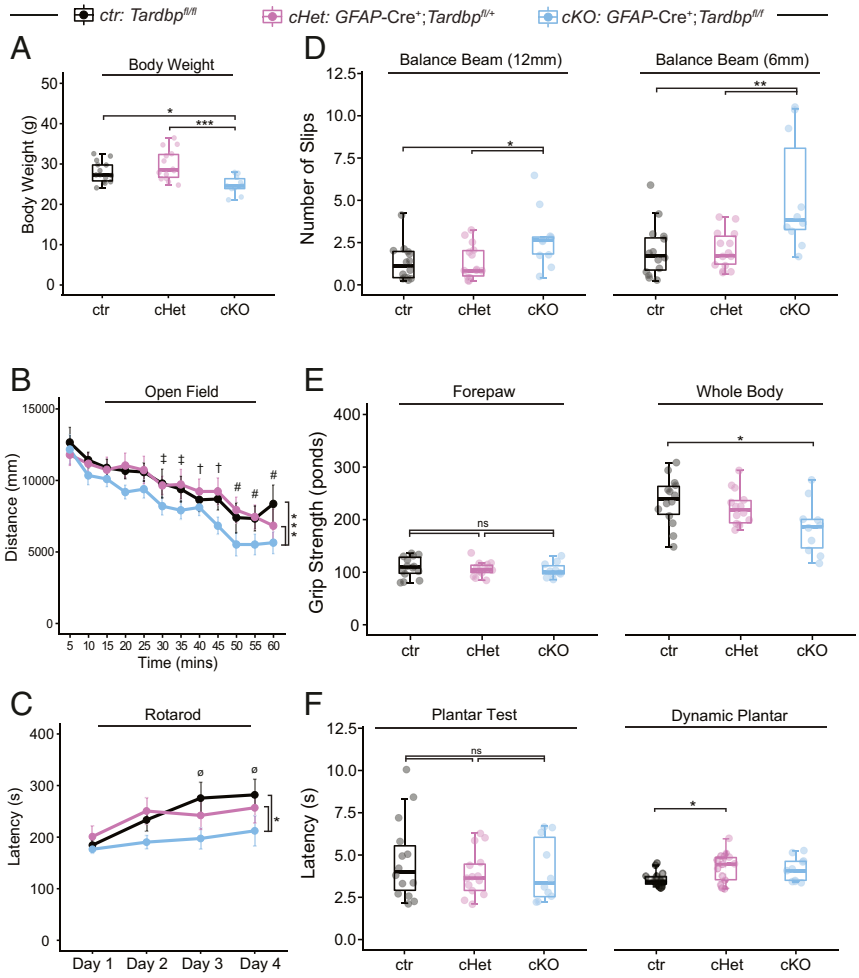

Fig. 7. Astroglial TDP-43–deleted mice develop motor, but not sensory, deficits. (*A*) Body weight measurements of *Tardbp*$^{fl/fl}$ (ctr), *GFAP-Cre*;*Tardbp*$^{fl/+}$ (cHet), *GFAP-Cre*;*Tardbp*$^{fl/fl}$ (cKO) mice at P90. *GFAP-Cre*;*Tardbp*$^{fl/fl}$ (cKO) mice exhibit a 10% reduction in body weight compared with control mice. ctr, $n = 14$; cHet, $n = 14$, cKO, $n = 10$. $^{*}P < 0.05$, $^{***}P < 0.001$. (*B–E*) Mice with astroglial TDP-43 deletion develop motor deficits. (*B*) Total distance traveled (in millimeters) in the open-field test. cKO mice showed reduced locomotor activity compared to controls. ctr, $n = 15$; cHet, $n = 14$, cKO, $n = 12$. $^{***}P < 0.001$, ‡significant difference from 5 min, †significant difference from 10 min, $^{\#}$significant difference from 15, 20, and 25 min. (*C*) Latency to fall in rotarod (in seconds) over 4 d of testing. cKO mice showed reduced ability in staying on the rotating rod compared to controls. ctr, $n = 14$; cHet, $n = 14$, cKO, $n = 10$. $^{*}P < 0.05$, ^{ø}significant difference from day 1. (*D*) Numbers of slips on balance beam tests, (*Left*) 12-mm beam, (*Right*) 6-mm beam. cKO mice have significantly more slips than controls when walking across the 12-mm and 6-mm beams. ctr, $n = 14$; cHet, $n = 14$, cKO, $n = 10$. $^{*}P < 0.05$, $^{**}P < 0.01$. (*E*) Grip strength of forepaw (*Left*) and whole body (*Right*) of ctr, cHet, cKO mice. Reduced grip strength was observed for the whole body, but not for the forepaw, in cKO mice. ctr, $n = 14$; cHet, $n = 14$, cKO, $n = 10$. $^{*}P < 0.05$. (*F*) cKO mice did not exhibit deficits in heat (Plantar test) or touch (Dynamic Plantar) sensitivity. $^{*}P < 0.05$, ns, not significant.

Because there is no apparent gender bias to the overserved pathology and molecular changes, female and male mice were included and randomly allocated to experimental groups according to age and genotype. To reduce the potential effects due to the estrus cycle of female mice, only male mice were used for the behavioral assays. All animals used in this study were between 2.5 and 3 mo of age. No animals or samples were excluded in any of the experiments.

Conditional TDP-43 (*Tardbp*$^{fl/fl}$) mice (stock no. 017591) and reporter *Rosa26*-GNZ mice (stock no. 008606) were purchased from the Jackson Laboratory. *GFAP*-Cre mice were described previously (43). For genotyping, genomic DNA was isolated from tail biopsies using salt-extraction methods and subjected to routine PCR methods using the following primers: *Tardbp*$^{fl/fl}$: 5′-ccctggctcatcaagaactg-3′ and 5′-tccaggacagccaggactac-3′; *GFAP*-Cre: 5′-ggggattcctcaactgacaa-3′ and 5′-catgtttagctggcccaaat-3′; and

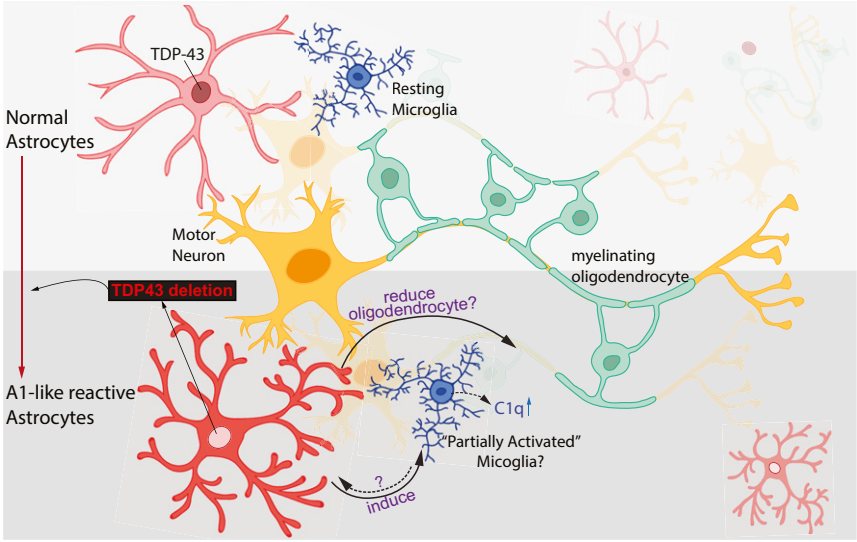

Fig. 8. Proposed working model of triglial dysfunction triggered by astroglial TDP-43 deletion. Astrocytes without TDP-43 show enhanced GFAP immunoreactivity and acquire an A1-reactive signature, which induces microglia to increase C1 complement system expression and leads to a reduction of mature oligodendrocytes.

Rosa26-GNZ: 5′-taagcctgcccagaagactc-3′, 5′-aaagtcgctctgagttgttat-3′ and 5′-tccagttcaacatcagccgctaca-3′.

Immunofluorescence, EdU Injection and Staining, Image Acquisition and Processing, Isolation of Astrocytes and Oligodendrocytes, and Immunoblotting. The detailed procedures are described in *SI Appendix* and the primary antibodies used in the study are listed in *SI Appendix*, Table S2.

RNA Analysis: qRT-PCR and RNA-Seq Analysis. Total RNA was extracted from spinal cord tissues of 3-mo-old mice and mRNA levels of genes of interest were determined by qRT-PCR. The detailed protocol can be found in *SI Appendix* and the list of primers used are listed in *SI Appendix*, Table S3. Further, multiplex strand specific RNA-seq libraries were prepared from the RNA using Illumina TruSeq RNA Sample Prep Kit. Four biological replicates were used for each genotype and the libraries were sequenced using Illumina HiSeq4000 pair-end 151-bp sequencing. Details of the bioinformatic analysis of the RNA-seq data, including alignment, abundance quantification, diagnostic plots, downstream functional analysis, and estimation of cell composition are provided in *SI Appendix*.

Behavioral Testing. The detail procedures for open field, balance beam, rotarod test, grip strength, plantar test for thermal sensation, and dynamic plantar test for mechanical sensation are described in detail in *SI Appendix*.

Statistics. For datasets with no repeated measures from individual mice (e.g., the behavior tests), we fit variance using linear models via analysis of variance (*aov* function in R) (70) to test the effect of the various variables on the respective responses. A Tukey's HSD test was used to contrast between genotypes of interest. When multiple measures from individual mice were observed (e.g., immunohistochemical data with $n = 3$ mice per genotype and 6 to 10 sections per mouse), we fit variance by linear mixed-effects models with fixed effects (such as genotype, region, time) and random effect of individual mice variation using the lme4 R package (71). The best linear mixed model (with the lowest AICc) (72) was selected and further pairwise contrasts were performed using Tukey's HSD test from the emmeans R package with Kenward–Roger approximations of degrees of freedom (73). Statistical analyses for the figures are included in Dataset S1. Whiskers in figures and values following the ± sign reflect SD.

Data Availability. The RNA-seq data reported in this paper have been deposited in the Gene Expression Omnibus database, https://www.ncbi.nlm.nih.gov/geo (accession no. GSE156542). All study data are included in the article and supporting information.

ACKNOWLEDGMENTS. The authors thank Dr. Edward Koo for sharing the confocal microscope; Dr. Fengwei Yu for sharing LacZ antibody; Xianiong Wang for assisting FACS; Jia Feng, Mandi See, Jiehao Wang, and Vivi Ding for their technical assistance; and all of the S.-C.L. laboratory members for support, discussion, and suggestions. The behavioral experiments were carried out at the Neuroscience Phenotyping Core Facility, which is supported by the National Medical Research Council–National University Health System Centre Grant–Neuroscience Phenotyping Core (NMRC/CG/M009/2017_NUH/NUHS). This work was supported by grants to S.-C.L. from the Swee Liew-Wadsworth Endowment fund, National University of Singapore, National Medical Research Council (NMRC/OFIRG/0001/2016 and NMRC/OFIRG/0042/2017), and Ministry of Education (MOE2016-T2-1-024), Singapore.

1. J. Sreedharan *et al*., TDP-43 mutations in familial and sporadic amyotrophic lateral sclerosis. *Science* **319**, 1668–1672 (2008).
2. E. Kabashi *et al*., TARDBP mutations in individuals with sporadic and familial amyotrophic lateral sclerosis. *Nat. Genet.* **40**, 572–574 (2008).
3. V. M. Van Deerlin *et al*., TARDBP mutations in amyotrophic lateral sclerosis with TDP-43 neuropathology: A genetic and histopathological analysis. *Lancet Neurol.* **7**, 409–416 (2008).
4. S. Lattante, G. A. Rouleau, E. Kabashi, TARDBP and FUS mutations associated with amyotrophic lateral sclerosis: Summary and update. *Hum. Mutat.* **34**, 812–826 (2013).
5. M. Neumann *et al*., Ubiquitinated TDP-43 in frontotemporal lobar degeneration and amyotrophic lateral sclerosis. *Science* **314**, 130–133 (2006).
6. T. Arai *et al*., TDP-43 is a component of ubiquitin-positive tau-negative inclusions in frontotemporal lobar degeneration and amyotrophic lateral sclerosis. *Biochem. Biophys. Res. Commun.* **351**, 602–611 (2006).
7. S.-C. Ling, M. Polymenidou, D. W. Cleveland, Converging mechanisms in ALS and FTD: Disrupted RNA and protein homeostasis. *Neuron* **79**, 416–438 (2013).
8. I. R. Mackenzie, R. Rademakers, M. Neumann, TDP-43 and FUS in amyotrophic lateral sclerosis and frontotemporal dementia. *Lancet Neurol.* **9**, 995–1007 (2010).
9. Z. Rohan, R. Matej, R. Rusina, G. G. Kovacs, Oligodendroglial response in the spinal cord in TDP-43 proteinopathy with motor neuron involvement. *Neurodegener. Dis.* **14**, 117–124 (2014).
10. R. H. Tan, Y. D. Ke, L. M. Ittner, G. M. Halliday, ALS/FTLD: Experimental models and reality. *Acta Neuropathol.* **133**, 177–196 (2017).
11. E. B. Lee, V. M.-Y. Lee, J. Q. Trojanowski, Gains or losses: Molecular mechanisms of TDP43-mediated neurodegeneration. *Nat. Rev. Neurosci.* **13**, 38–50 (2011).
12. S. H. Ou, F. Wu, D. Harrich, L. F. García-Martínez, R. B. Gaynor, Cloning and characterization of a novel cellular protein, TDP-43, that binds to human immunodeficiency virus type 1 TAR DNA sequence motifs. *J. Virol.* **69**, 3584–3596 (1995).
13. C. Lagier-Tourenne, M. Polymenidou, D. W. Cleveland, TDP-43 and FUS/TLS: Emerging roles in RNA processing and neurodegeneration. *Hum. Mol. Genet.* **19**, R46–R64 (2010).
14. S.-C. Ling, Synaptic paths to neurodegeneration: The emerging role of TDP-43 and FUS in synaptic functions. *Neural Plast.* **2018**, 8413496 (2018).
15. H. Ederle, D. Dormann, TDP-43 and FUS en route from the nucleus to the cytoplasm. *FEBS Lett.* **591**, 1489–1507 (2017).
16. N. H. Alami *et al*., Axonal transport of TDP-43 mRNA granules is impaired by ALS-causing mutations. *Neuron* **81**, 536–543 (2014).
17. P. Majumder, J.-F. Chu, B. Chatterjee, K. B. S. Swamy, C. J. Shen, Co-regulation of mRNA translation by TDP-43 and Fragile X syndrome protein FMRP. *Acta Neuropathol.* **132**, 721–738 (2016).
18. N. Neelagandan *et al*., TDP-43 enhances translation of specific mRNAs linked to neurodegenerative disease. *Nucleic Acids Res.* **314**, 130–21 (2018).
19. W. Wang *et al*., The inhibition of TDP-43 mitochondrial localization blocks its neuronal toxicity. *Nat. Med.* **22**, 869–878 (2016).
20. J. K. Bose, C.-C. Huang, C.-K. J. Shen, Regulation of autophagy by neuropathological protein TDP-43. *J. Biol. Chem.* **286**, 44441–44448 (2011).
21. Q. Xia *et al*., TDP-43 loss of function increases TFEB activity and blocks autophagosome-lysosome fusion. *EMBO J.* **35**, 121–142 (2016).
22. A. Roczniak-Ferguson, S. M. Ferguson, Pleiotropic requirements for human TDP-43 in the regulation of cell and organelle homeostasis. *Life Sci. Alliance* **2**, e201900358 (2019).
23. Y. Zhang *et al*., An RNA-sequencing transcriptome and splicing database of glia, neurons, and vascular cells of the cerebral cortex. *J. Neurosci.* **34**, 11929–11947 (2014).
24. N. J. Allen, B. A. Barres, Neuroscience: Glia—More than just brain glue. *Nature* **457**, 675–677 (2009).
25. S. A. Liddelow, B. A. Barres, Reactive astrocytes: Production, function, and therapeutic potential. *Immunity* **46**, 957–967 (2017).
26. K. L. Adams, V. Gallo, The diversity and disparity of the glial scar. *Nat. Neurosci.* **21**, 9–15 (2017).
27. M. A. Anderson *et al*., Astrocyte scar formation aids central nervous system axon regeneration. *Nature* **532**, 195–200 (2016).
28. S. A. Liddelow *et al*., Neurotoxic reactive astrocytes are induced by activated microglia. *Nature* **541**, 481–487 (2017).
29. Y. Shi *et al*.; Alzheimer's Disease Neuroimaging Initiative, ApoE4 markedly exacerbates tau-mediated neurodegeneration in a mouse model of tauopathy. *Nature* **549**, 523–527 (2017).
30. S. P. Yun *et al*., Block of A1 astrocyte conversion by microglia is neuroprotective in models of Parkinson's disease. *Nat. Med.* **24**, 931–938 (2018).
31. E. M. Gibson *et al*., Methotrexate chemotherapy induces persistent tri-glial dysregulation that underlies chemotherapy-related cognitive impairment. *Cell* **176**, 43–55.e13 (2019).
32. H. Ilieva, M. Polymenidou, D. W. Cleveland, Non-cell autonomous toxicity in neurodegenerative disorders: ALS and beyond. *J. Cell Biol.* **187**, 761–772 (2009).
33. A. M. Haidet-Phillips *et al*., Astrocytes from familial and sporadic ALS patients are toxic to motor neurons. *Nat. Biotechnol.* **29**, 824–828 (2011).
34. K. Meyer *et al*., Direct conversion of patient fibroblasts demonstrates non-cell autonomous toxicity of astrocytes to motor neurons in familial and sporadic ALS. *Proc. Natl. Acad. Sci. U.S.A.* **111**, 829–832 (2014).
35. K. Qian *et al*., Sporadic ALS astrocytes induce neuronal degeneration in vivo. *Stem Cell Reports* **8**, 843–855 (2017).
36. J. Tong *et al*., Expression of ALS-linked TDP-43 mutant in astrocytes causes non-cell-autonomous motor neuron death in rats. *EMBO J.* **32**, 1917–1926 (2013).
37. F. Rojas, N. Cortes, S. Abarzua, A. Dyrda, B. van Zundert, Astrocytes expressing mutant SOD1 and TDP43 trigger motoneuron death that is mediated via sodium channels and nitroxidative stress. *Front. Cell. Neurosci.* **8**, 24 (2014).
38. A. Serio *et al*., Astrocyte pathology and the absence of non-cell autonomy in an induced pluripotent stem cell model of TDP-43 proteinopathy. *Proc. Natl. Acad. Sci. U.S.A.* **110**, 4697–4702 (2013).
39. A. M. Haidet-Phillips *et al*., Altered astrocytic expression of TDP-43 does not influence motor neuron survival. *Exp. Neurol.* **250**, 250–259 (2013).
40. S. H. Kang *et al*., Degeneration and impaired regeneration of gray matter oligodendrocytes in amyotrophic lateral sclerosis. *Nat. Neurosci.* **16**, 571–579 (2013).
41. J. Wang *et al*., Cell-autonomous requirement of TDP-43, an ALS/FTD signature protein, for oligodendrocyte survival and myelination. *Proc. Natl. Acad. Sci. U.S.A.* **115**, E10941–E10950 (2018).
42. R. C. Paolicelli *et al*., TDP-43 depletion in microglia promotes amyloid clearance but also induces synapse loss. *Neuron* **95**, 297–308.e6 (2017).
43. M. L. Bajenaru *et al*., Astrocyte-specific inactivation of the neurofibromatosis 1 gene (NF1) is insufficient for astrocytoma formation. *Mol. Cell. Biol.* **22**, 5100–5113 (2002).
44. J. Z. Stoller *et al*., Cre reporter mouse expressing a nuclear localized fusion of GFP and β-galactosidase reveals new derivatives of Pax3-expressing precursors. *Genesis* **46**, 200–204 (2008).
45. M. Polymenidou *et al*., Long pre-mRNA depletion and RNA missplicing contribute to neuronal vulnerability from loss of TDP-43. *Nat. Neurosci.* **14**, 459–468 (2011).

46. Y. M. Ayala *et al*., TDP-43 regulates its mRNA levels through a negative feedback loop. *EMBO J.* **30**, 277–288 (2011).
47. J. L. Zamanian *et al*., Genomic analysis of reactive astrogliosis. *J. Neurosci.* **32**, 6391–6410 (2012).
48. D. Brites, A. R. Vaz, Microglia centered pathogenesis in ALS: Insights in cell interconnectivity. *Front. Cell. Neurosci.* **8**, 117 (2014).
49. V. Chhor *et al*., Characterization of phenotype markers and neuronotoxic potential of polarised primary microglia in vitro. *Brain Behav. Immun.* **32**, 70–85 (2013).
50. W. Zhao, D. R. Beers, S. H. Appel, Immune-mediated mechanisms in the pathoprogression of amyotrophic lateral sclerosis. *NeuroImmune Pharmacol.* **8**, 888–899 (2013).
51. M. C. Evans, Y. Couch, N. Sibson, M. R. Turner, Inflammation and neurovascular changes in amyotrophic lateral sclerosis. *Mol. Cell. Neurosci.* **53**, 34–41 (2013).
52. M. V. Sofroniew, H. V. Vinters, Astrocytes: Biology and pathology. *Acta Neuropathologica* **119**, 7–35 (2010).
53. D. Tsoucas *et al*., Accurate estimation of cell-type composition from gene expression data. *Nat. Commun.* **10**, 2975 (2019).
54. X. Han *et al*., Mapping the Mouse Cell Atlas by microwell-seq. *Cell* **172**, 1091–1107.e17 (2018).
55. M. Traka *et al*., A genetic mouse model of adult-onset, pervasive central nervous system demyelination with robust remyelination. *Brain* **133**, 3017–3029 (2010).
56. C. C. Stolt *et al*., Terminal differentiation of myelin-forming oligodendrocytes depends on the transcription factor Sox10. *Genes Dev.* **16**, 165–170 (2002).
57. C. Yang *et al*., Partial loss of TDP-43 function causes phenotypes of amyotrophic lateral sclerosis. *Proc. Natl. Acad. Sci. U.S.A.* **111**, E1121–E1129 (2014).
58. L. Li *et al*., GFAP mutations in astrocytes impair oligodendrocyte progenitor proliferation and myelination in an hiPSC model of Alexander disease. *Cell Stem Cell* **23**, 239–251.e6 (2018).
59. A. K. Walker *et al*., Astrocytic TDP-43 pathology in Alexander disease. *J. Neurosci.* **34**, 6448–6458 (2014).
60. J. Cai *et al*., A crucial role for Olig2 in white matter astrocyte development. *Development* **134**, 1887–1899 (2007).
61. L. Luo *et al*., Optimizing nervous system-specific gene targeting with Cre driver lines: Prevalence of germline recombination and influencing factors. *Neuron* **106**, 37–65.e5 (2020).
62. A. Uchino *et al*., Incidence and extent of TDP-43 accumulation in aging human brain. *Acta Neuropathol. Commun.* **3**, 35 (2015).
63. S. Nag *et al*., TDP-43 pathology and memory impairment in elders without pathologic diagnoses of AD or FTLD. *Neurology* **88**, 653–660 (2017).
64. K. A. Josephs *et al*., TDP-43 is a key player in the clinical features associated with Alzheimer's disease. *Acta Neuropathol.* **127**, 811–824 (2014).
65. K. A. Josephs *et al*., Staging TDP-43 pathology in Alzheimer's disease. *Acta Neuropathol.* **127**, 441–450 (2014).
66. J. Siuda, S. Fujioka, Z. K. Wszolek, Parkinsonian syndrome in familial frontotemporal dementia. *Parkinsonism Relat. Disord.* **20**, 957–964 (2014).
67. N. Aoki *et al*., Hippocampal sclerosis in Lewy body disease is a TDP-43 proteinopathy similar to FTLD-TDP Type A. *Acta Neuropathol.* **129**, 53–64 (2015).
68. S. Nag *et al*., Hippocampal sclerosis and TDP-43 pathology in aging and Alzheimer disease. *Ann. Neurol.* **77**, 942–952 (2015).
69. P. T. Nelson *et al*., Limbic-predominant age-related TDP-43 encephalopathy (LATE): Consensus working group report. *Brain* **142**, 1503–1527 (2019).
70. R Core Team, *R: A Language and Environment for Statistical Computing* (R Foundation for Statistical Computing, 2019).
71. D. Bates, M. Mächler, B. Bolker, S. Walker, Fitting linear mixed-effects models using lme4. *J. Stat. Softw.* **67**, 1–48 (2015).
72. M. J. Mazerolle, AICcmodavg: Model Selection and Multimodel Inference Based on (Q) AIC(c), https://CRAN.R-project.org/package=AICcmodavg (2019). Accessed 4 April 2020.
73. R. Lenth, H. Singmann, J. Love, P. Buerkner, M. Herve, emmeans: Estimated Marginal Means, aka Least-Squares Means, https://CRAN.R-project.org/package=emmeans (2020). Accessed 4 April 2020.